Mean Atomic Number Quantitative Assessment in Backscattered Electron Imaging

E. Sánchez,[1] M. Torres Deluigi,[2] and G. Castellano[3,*]

[1]INQUISAL, Universidad Nacional de San Luis, San Luis, Argentina
[2]Departamento de Física, INQUISAL, Universidad Nacional de San Luis, San Luis, Argentina
[3]FaMAF, Universidad Nacional de Córdoba, Córdoba, Argentina

Abstract: A method for obtaining quantitative mean atomic number images in a scanning electron microscope for different kinds of samples has been developed. The backscattered electron signal is monotonically increasing with the mean atomic number Z, and accordingly Z can be given as a function of the image gray levels. From results obtained from Monte Carlo simulations, an exponential function is fitted to convert the backscattered registered gray levels into a Z image map. Once this fitting was performed, the reproducibility of the Z determination was checked through the acquisition of backscattered electron images from metal and mineral standards. The developed method can be applied to any unknown sample, always controlling the experimental conditions, as shown here for a thin section of a rock in which several unknown mineral phases are present; the results obtained herein are compared to quantitative assessments performed with X-ray spectra from each mineral phase.

INTRODUCTION

Backscattered electron images (BEI) are quite valuable in different areas of materials characterization because they provide important information about the mean atomic number of the samples under study (Goldstein et al., 1992). This signal is built up with electrons that mainly undergo elastic interactions with the specimen atoms and escape from the entering surface, their energy distribution being somewhat peaked with a maximum quite close to the incident energy. The lower limit of 50 eV is conventionally defined as the threshold for discriminating the detection of secondary electrons, which mostly have a much lower energy distribution peaked around 3 eV; this alternative signal is typically used to furnish topographical images and does not exhibit a strong dependence on the sample mean atomic number. The backscattered electron coefficient η is defined as the ratio of the number of backscattered electrons n_{BSE} to the total number of incident electrons n_B:

$$\eta = n_{BSE}/n_B. \tag{1}$$

The value of this coefficient is sensitive to changes in the mean atomic number Z of the irradiated sample, showing a monotonically increasing dependence (Reed, 1993), which means that if this behavior is adequately known, the gray-scale BEI could readily be converted into Z images.

The conventional external detector for backscattered electrons in a scanning electron microscope (SEM) is located around the polar piece, right above the irradiated sample. This takes advantage of the fact that for zero surface tilt this signal is maximum at this position because the backscattered electron intensity obeys a cosine distribution when referred to the surface normal direction (Goldstein et al., 1992). It is important to bear in mind that if BEIs are intended to reliably survey the sample average atomic number Z, the incident beam current must be maintained really steady through all the images acquired because the η signal will vary proportionally. The same caution must be taken in controlling the brightness, contrast, detector gain, and scanning speeds, which may distort the gray-level values in the image registered. If for some reason this is not possible, the acquired images must be normalized with the beam current used for each frame registered.

The importance of BEIs lies in the fact that they are widely used in a variety of scientific or technological investigations, such as chemical geology, cement investigations, art and cultural heritage pieces, hard tissue characterization, etc. (Roschger et al., 1998; Ginibre et al., 2002; Kjellsen et al., 2003; Schalm et al., 2003; Triebold et al., 2006; Galván Josa et al., 2009; Peters, 2009; Keune et al., 2011). In all these studies some relationship between the BE signal and Z is used, and in some exceptional cases a fit is attempted to transform BEIs into Z images. However, no systematic study has been done so far, which provides a means of obtaining this kind of relationship routinely for a wide atomic number range. The conversion of BE signal into semiquantitative Z is nontrivial, and it is important to stress that the information offered by a Z image is more valuable than the original BEI. A mean atomic number map allows one to readily identify mineral phases in it, producing a rapid and efficient analysis. In cases where only two phases are present in a solid solution (Ginibre et al., 2002; Triebold et al., 2006), the Z map straightforwardly permits a concentration map.

Harding (2002) gave an interesting approach for the identification of mineral phases in a specimen that is based on BEI. Nevertheless, we assert that the precise relationship between the measured intensity of backscattered electrons in a SEM and the average atomic number of the specimen is still argued.

In this work a methodology for furnishing quantitative mean atomic number images has been developed that is applicable not only to mineral samples but also for any inhomogeneous material, e.g., alloys in which microphases give different properties to the material. The method is intended to be valid in a wide range of materials and to describe accurately the phases of low Z. As a first step, this approach has been tested at low magnification (analyzed area 40 μm $\times$ 30 μm) to guarantee sample homogeneity but can readily be used in samples observed at higher magnifications. These Z images were possible by fitting a set of η results from Monte Carlo simulations with a simple exponential function, so that the backscattered electron signal is transformed to Z gray levels with the corresponding scaling adjustment. Once this fitting was performed, the reproducibility of the Z determination was checked through the acquisition of BEI from metal and mineral standards, carefully controlling the experimental conditions.

Finally, images from a thin section of a rock were acquired in which several mineral unknown phases are present. To transform η to Z values, the function fitted to the set of Monte Carlo backscattered coefficients was used, as well as measurements from two additional standards, which are necessary for a global scaling calibration. A routine in MATLAB® was written, which transforms η to Z values using the function fitted. An artificial coloring option is available to facilitate the visualization of the Z contrast. The results obtained through the methodology developed here are compared to quantitative assessments performed with X-ray spectra from each mineral phase.

Monte Carlo Simulations

The general behavior of η as a function of Z has been documented in the literature through different approaches (Goldstein et al., 1992). Several expressions have also been given to describe this behavior, some analytical formulae being available (see for example Reuter, 1972 or Joy, 1991).

These functions adequately describe the dependence of η with Z, with a similar behavior in all the Z range for $E = 20$ keV, as shown in Figure 1. However, these expressions cannot be inverted to reobtain Z values from a BEI. For this reason, Monte Carlo simulations for the backscattering coefficient were performed using the PENELOPE routine package (Salvat et al., 2003) because the scattering properties of materials have successfully been described with it (Acosta et al., 1996, 1998, 2002; Llovet et al., 2003; Sempau et al., 2003). These simulations were performed for a set of metal and mineral standards covering a range $2.74 \leq Z \leq 82$.

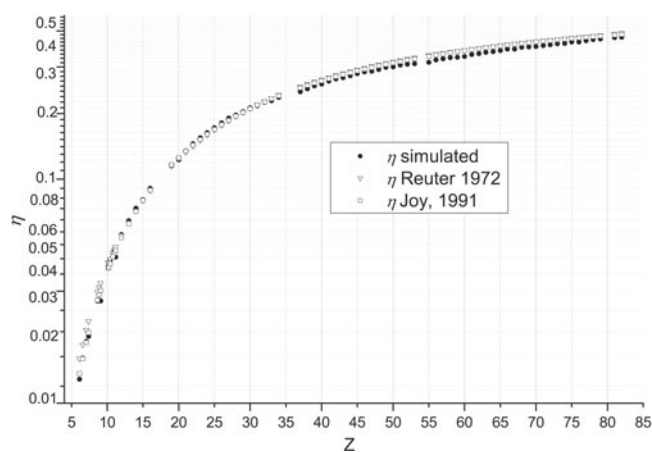The Monte Carlo code PENELOPE (PENetration and Energy LOss of Positrons and Electrons) simulates the trans-

Figure 1. η as a function of Z for Monte Carlo simulations, as well as those predicted with the expressions by Reuter (1972) and Joy (1991) for an incident energy of 20 keV.

port of electrons, positrons, and photons in arbitrary material systems consisting of homogeneous regions separated by well-defined interfaces. Interactions are appropriately described for quite a wide energy range, from a few hundred eV to 1 GeV. The scattering simulation algorithm combines accurate models for the different interaction processes with numerical databases (Salvat et al., 2003). For the case of positrons and electrons, tracks can be assessed through a "mixed" scheme, which combines the detailed simulation of hard events (with important angular deflection or energy loss) with condensed simulation of soft events, which are grouped in a single interaction (multiple scattering).

The simulations were performed in this work using the sample main program PENSLAB of the 2003 distribution. This program deals with a very simple geometry involving a flat material block of uniform thickness, and the lateral extension is assumed infinite compared to the electron range in the material involved. Primary electrons are emitted from a point source with a single energy, the incident energy E_0. In the simulations presented here, the thickness was taken large enough to ensure no electrons were transmitted through the sample, the incident energy value chosen was 20 keV, and the number of primary tracks was always set to guarantee a statistical uncertainty of 1% or below. It should be emphasized that since η slightly depends on E_0, similar expressions should be obtained if different incident energies are involved.

EXPERIMENTAL

For the validation of the model proposed here, BEIs were acquired in a LEO 1450VP SEM (Leoco Corporation, China) furnished with a scintillator for the detection of secondary electrons and a four-quadrant solid-state diode backscattered electron detector, from the Laboratorio de Microscopía Electrónica y Microanálisis (LABMEM) of the Universidad Nacional de San Luis, Argentina. X-rays can also be registered by means of an EDAX Genesis 2000 (EDAX, Mah-

wah, NJ, USA) energy dispersive spectrometer (EDS) with a polypropilene ultrathin window Si(Li) detector and an INCA WAVE 700 (Oxford Instruments, Abingdon, Oxfordshire, UK) wavelength dispersive spectrometer with different crystals. For the present work, the EDS was used, as detailed below.

Backscattered electron signals were measured in a set of 34 metals with a wide atomic number range ($12 \leq Z \leq 76$), always maintaining the same experimental conditions, whereas a second group of measurements was performed for 26 standard mineral samples with $10.41 \leq Z \leq 73.16$. To this aim, commercial metal and mineral standards SPI #02751-AB and SPI #02753-AB, respectively, were used.

BEIs were acquired checking the probe current in each experiment by means of a Faraday cup attached to the set of metal and mineral standards, selecting the incident energy, as well as brightness and contrast values to efficiently observe the whole range of Z involved. The experimental conditions were therefore 0.85 nA probe current, 41.7% image brightness, 42.2% image contrast, 20 keV incident electron energy, 15 mm working distance, 40 μm $\times$ 30 μm analyzed areas, and 20.13 s full screen rastering speed. It is important to recall that although the measurement series were taken in different days, care was taken to preserve the experimental conditions in each case.

With the aim of testing the methodology proposed here, a rock thin section was studied for which the BEI exhibited several mineral phases of different gray levels. Under the same experimental conditions, four mineral standards were also measured in this opportunity, which covered the whole Z range appearing in this thin section (see Table 2 later in this article). In this case the values for brightness and contrast were 40.9% and 83.3%, respectively, whereas the probe current was 0.26 nA. Low magnifications were chosen to avoid possible fluctuations in sample homogeneities. EDS X-ray spectra were also acquired from 10 different mineral regions of this rock thin sample and from 12 mineral standards to perform a quantification that allowed the validation for the mean atomic numbers found with the methodology proposed here. To this aim, point analysis was chosen in the SEM and recorded during a live time of 200 s, detector dead time being always below 17%.

Results and Discussion

Figure 1 shows a comparison between the expressions given by Reuter, Joy, and the Monte Carlo results for the backscattering coefficient. It can be seen that in the range $11 \leq Z \leq 35$, all the η values are in very good agreement; outside this range, minor differences occur. Since for Z greater than 35 only slight differences between simulated and calculated values are observed, a set of simulated η values for $10 \leq Z \leq 76$ will be considered to find an expression that converts backscattered gray levels into Z values. It is worth mentioning that the backscattering cross section presents discontinuities as long as electronic shell orbitals are com-
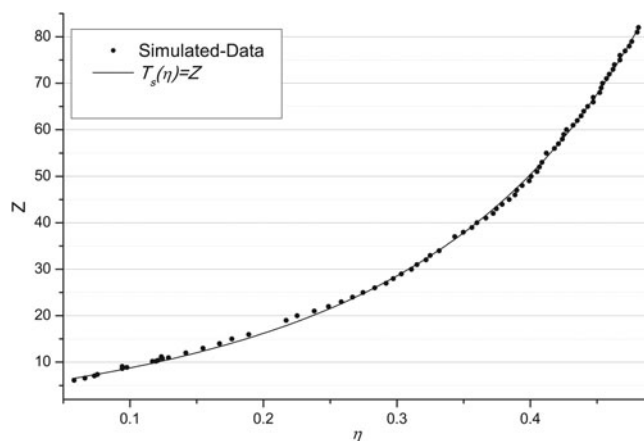

Figure 2. Z as a function of η, as obtained from the fit of equation (2).

pleted. The expressions developed here are devoted to mean atomic numbers in multielemental samples, where this effect is washed out.

The data associated with the set of standards for the backscattering coefficient obtained through Monte Carlo simulations with PENELOPE (Fig. 2) were fitted with different options, the most convenient for the present purposes being

$$T_s(\eta) = Z = Z_0 + A \cdot \exp[(\eta - \eta_0)^b/t], \qquad (2)$$

where Z_0, A, η_0, b, and t are the searched parameters. The values obtained through this fitting are $Z_0 = -30.02$, $t = 50{,}330$, $A = 25.17$, $\eta_0 = -2.699$, and $b = 9.7039$. The fit is shown in Figure 2 along with the original simulated data. It can be seen that only slight differences are observed for extremely low mean atomic numbers; however, this region is out of interest in typical studies of this kind.

Since the images obtained should correspond to homogeneous gray levels, the value associated to each region was taken as the maximum population 8-bit gray level in the intensity histogram. Each gray level I must correspond to a definite Z value when calibrating with the standard set measurement. However, as shown in Figure 3, when comparing measurements made at different times (the metal set was measured first, another day was devoted to the set "Minerals 1" in Fig. 3, and a third measurement was carried out on the set "Minerals 2" in Fig. 3), it can clearly be seen that although the experimental conditions were maintained through the three sets of measurements, the intensities I are not correlated to a unique Z value. This is due to the inability to rigorously control the stability of electronic components such as the analogue signal amplifier of the backscattered electron detector, the brightness and contrast in the final image scanning, and other electronic components introducing instabilities that inhibit exactly reproducing experimental conditions. These random drifts usually will not affect an ordinary BEI acquisition but have to be taken into account when a quantitative determination of Z is sought. This fact implies that for each measurement carried out, a different transform function $T(\eta)$ must be
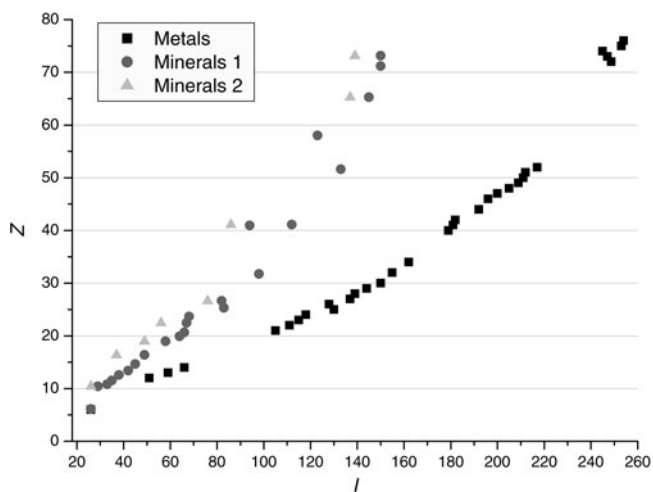
Figure 3. Z values associated with the different standard measurement sets for the backscattered gray levels I.

determined, by using a reduced set of samples of known mean atomic number.

The BEIs in the SEM are built up from the signals generated in the backscattered electron detector. These signals correspond to voltage differences proportional to the amount of electrons interacting in the detector. These voltage signals are spread in a given range so as to allow the observation of a pixel of certain intensity I in the image registered, which can be conveniently modified through additive constants or gray-level scaling. These two operations define respectively the brightness and contrast for each measurement, so that the relationship between I with η may be written as

$$I(Z) = C \cdot \eta(Z) + B, \qquad (3)$$

where C and B represent the contrast and brightness factors. To have Z as a function of I, the dependence of η as a function of Z was found in a first stage, which means inverting the function $T_s(\eta)$ given in equation (2). The exponential dependence chosen makes this mathematical operation easy, obtaining in this way

$$(T_s)^{-1} \equiv \eta(Z) = \eta_0 + \{t \cdot \ln[(Z - Z_0)/A]\}^{1/b}. \qquad (4)$$

By assessing this expression for the different Z values for the standards, and relating these values with the corresponding I values, a linear relationship was found, obtaining through this procedure the constants C and B of equation (4). Finally, the function $I(Z)$ was inverted, achieving the desired relationship of Z as a function of I:

$$Z \equiv T(I) = Z_0 + A \cdot \exp\{[((I - B)/C - \eta_0)^b]/t\}. \qquad (5)$$

For the three measurement series, the corresponding linear fits were performed, thus obtaining the B and C factors for each case. The results of these fittings are displayed in Table 1, along with the corresponding value for the correlation coefficient R^2 (Steel & Torrie, 1960). In Figure 4, the comparisons between the experimental and fitted values are displayed. In the case of the metal standard set, the largest percent difference was 5.5% for $Z = 52$, whereas for the

Table 1. Results for the Parameters B, C, and R^2 from the Fittings of Backscattered Intensities I as a Function of η for the Different Measurements in Metal and Mineral Standards.

Measurement Set	B	C	R^2
Metals	−49.98109	694.01092	0.996
Minerals 1	−21.41626	370.46994	0.993
Minerals 2	−29.78984	356.09712	0.957

remainder this difference was below 4.6%. For the first mineral measurement set, the agreement is similar with a few exceptions around 6.1% to 7.7%, whereas the second set of mineral measurements showed a similar agreement, also with a few exceptions presenting stronger discrepancies. It must be emphasized here that collective effects, such as crystalline or channeling response, are not taken into account in this study; this kind of behavior could increase the backscattering signal independently of the sample mean atomic number (Reimer, 1993). The similar values obtained for R^2 show reasonable values for the three fits.

APPLICATION: QUANTITATIVE Z IMAGE FOR A THIN ROCK SAMPLE

The measurements for the four minerals mentioned at the end of the Results and Discussion section for the assessment of the fitting function $T(I)$ were taken into account again, using the procedure described in the previous section. In this case, repeated measurements for the intensities were performed in all four minerals to verify that no variations in the successive measured I values were noticeable. Calculations were therefore performed using the I values displayed in Table 2. The parameters produced by this fitting were $B = -173.61$ and $C = 1,643.81$, with an R^2 value of 0.993.

By replacing the values for B and C in equation (5), the corresponding $T(I)$ function was again obtained, and this was used in the MATLAB® routine written for image processing. As a first step, this routine transforms the 1024 × 764 BE image in a matrix in which each element represents the individual gray-level intensity for each pixel. The function $T(I)$ is then applied to these matrix elements, transforming each I to a Z value. The resulting Z values are then stretched to an optimum dynamic range in an 8-bit image, i.e., from 0 to 255 in a gray-level scale. This monochrome image can also be converted to a 1024 × 764 color image, only for ease of visualization purposes, as shown below.

The BE image processed was obtained for an unknown thin-section rock sample that exhibits different mineral phases, as displayed in Figure 5. For the largest and most relevant phases, X-ray spectra were acquired from the 10 points labeled in this figure. With the corresponding characteristic intensities taken in standard samples, the concentrations for the elements present in these points were obtained. To this aim, the built-in program EDAX Genesis® was used. Through this procedure, values for the mean atomic numbers Z_X were assessed in each of the points selected, which were afterward contrasted with the corresponding Z_T values
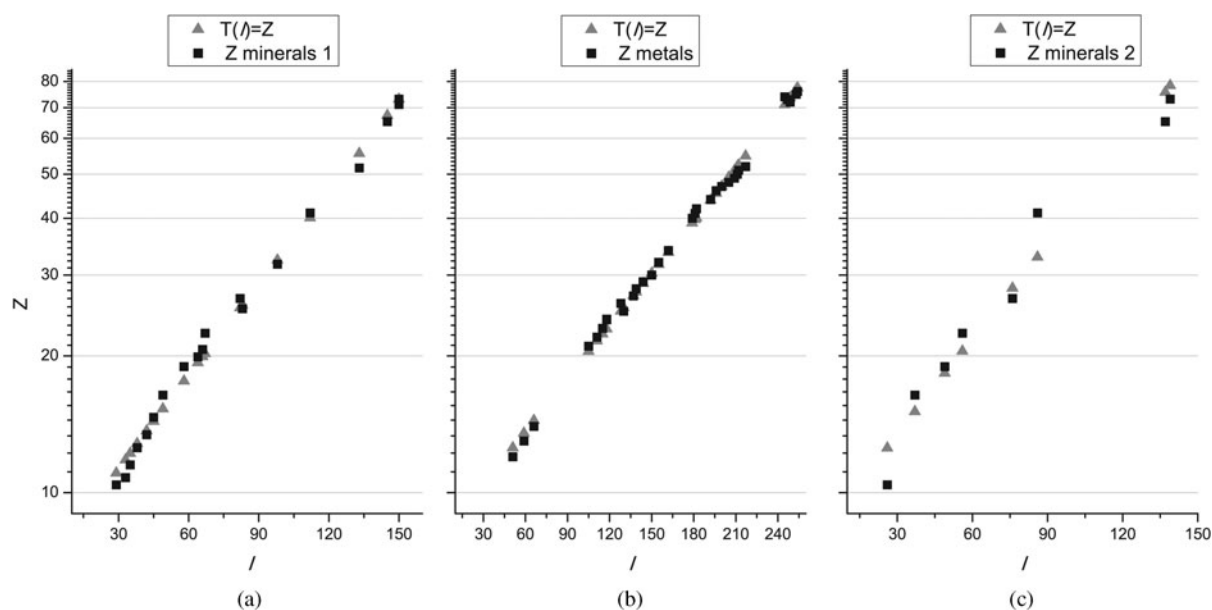
Figure 4. Comparison of the fitting $T(I)$ achieved for Z as a function of measured I: (**a**) mineral standard set #1; (**b**) metal standard set; (**c**) mineral standard set #2.

Table 2. Z and I Values for the BE Images for a 73 μm $\times$ 55 μm Analyzed Area in the Four Standard Mineral Samples.*

Standard Mineral	Z	I	Z_T	% Difference
Periclase	10.41	40	10.64	-2.20
Calcite	12.56	77	12.23	2.64
Fluorite	14.65	126	14.62	0.23
Hematite	20.59	226	20.75	-0.77

*Estimated Z_T values are also shown, as obtained with the T function evaluated in the corresponding I values. Percent differences between Z and Z_T are also shown.

obtained from the BE average values I, as transformed through the function $T(I)$.

Figure 6 displays a comparison between the real mean atomic numbers against the Z_T values produced from BE intensities and the Z_X obtained from X-ray analysis. In the comparison among standards, the Z and Z_T values are almost equivalent because the fitting of the Z_T values is achieved by using the standard values for Z. The Z_X values are slightly greater than the corresponding Z_T, the difference being slightly larger for $I = 180$ (which corresponds to point 3 of Fig. 5) and $I = 252$ (points 1, 5, and 9 of Fig. 5).

From Figure 6, it can be observed that the approach proposed here provides reasonable results, with uncertainties that are comparable with those produced from the EDS quantifications (a few percent). Points 1, 5, and 9 exhibit slightly greater differences between Z_T and Z_X, though always within the differences observed among the mineral standards, as shown above (Fig. 4). The quantitative image of Figure 7, which was obtained from Figure 5, therefore produces mean atomic numbers for each phase with an appropriate uncertainty for most phases, which allows the observation of the spatial distribution for Z values and the

identification of the corresponding phases. Compared to the "correct" mean atomic numbers corresponding to these phases, the small differences in Z may be due to water remainders, which were not included in the EDS analysis, producing slightly greater Z values.

The five phases found are unambiguously discriminated through this procedure: quartz ($Z = 10.5$; point 4); cordierite ($Z = 12.4$; point 8), almandine garnet ($Z = 13.4$; point 7), Ti-rich illmenite ($Z = 17.6$; points 3, 6, 10), Fe-rich illmenite ($Z = 19$; point 2), and zircon ($Z = 23$; points 1, 5, 9). It is noteworthy that through this method the quantitative Z image permits not only different phases to be distinguished, but it also allows the accurate discrimination of phases slightly differing in their composition, as is the case of points 2 and 3 of Figure 7. The high sensitivity achieved in these quantitative Z images is a clear consequence of the use of the Monte Carlo η values produced for a very wide range of samples ($2.74 \leq Z \leq 82$).

Conclusion

Monte Carlo simulations with the PENELOPE package allowed us to obtain an adequate description of the backscattered electron signal as a function of the mean atomic number Z, in the range $10 \leq Z \leq 76$. This behavior was experimentally corroborated by measurements in metal and mineral standards. The relationship found was implemented in a program written in MATLAB® environment, which allows us to obtain quantitative images of Z values. In this work, this procedure was exemplified by applying it to a thin-section rock sample, for which the different phases are clearly identified; appropriate Z values were assessed for each phase, as compared to quantitative analyses accomplished with the EDS system attached to the SEM used. This example supports the methodology proposed here for the assessment of quantita-
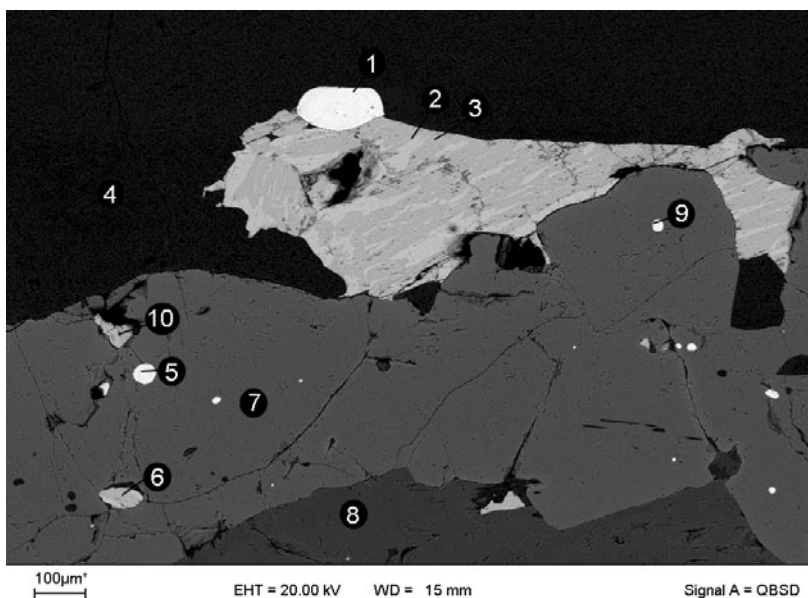
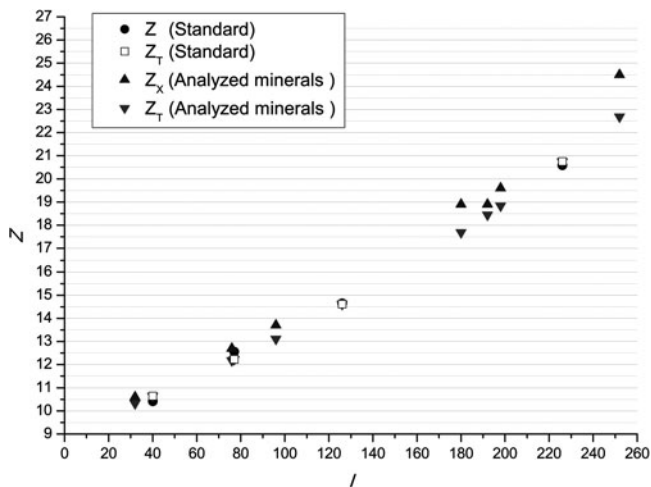**Figure 5.** BE image for the thin-section rock sample used; analyzed area 1,600 μm $\times$ 1,200 μm.

Figure 6. Comparison of the real mean atomic numbers Z and those produced from BE intensities (Z_T) and from X-ray analysis (Z_X).

Figure 7. Artificial color scaled quantitative mean atomic number image for the thin-section rock sample used; analyzed area: 1,600 μm $\times$ 1,200 μm.

tive Z images in an SEM, which may suffice in different analytical situations such as phase identification, particle discrimination, or the characterization of microstructures.

The success of the results obtained through this approach strongly depends on the care taken in the experimental conditions through the different steps accomplished. For an efficient use of this method, different parameters must be maintained constant, such as the scanning speed, brightness, contrast, accelerating voltage, and working distance; any change in these parameters will alter the backscattered electron signal, which inhibits their direct comparison, as has been performed here. Focus must also be adequately controlled because the backscattered electron intensity measured may be scaled in an uncontrolled way. Magnification values instead may arbitrarily be changed as long as the beam current and working distance remain unaltered.
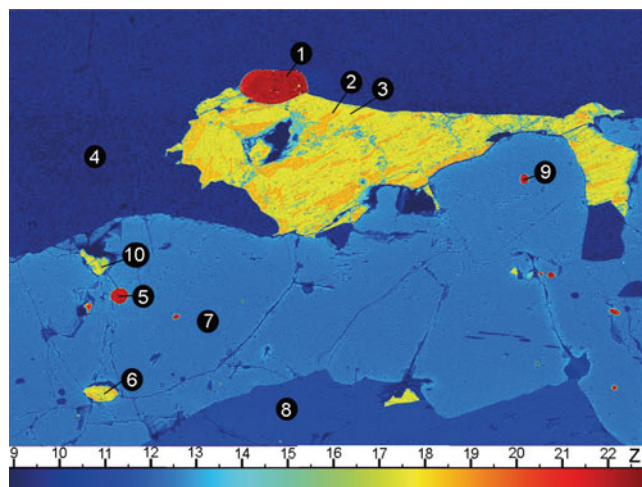
To guarantee an appropriate determination of the function $T(I)$, standards with extreme Z values must be measured during the calibration process. Obviously, better fittings are achieved when the number of standards used is high enough to reduce the uncertainties of the parameters of the function $T(I)$.

REFERENCES

ACOSTA, E., COLEONI, E., CASTELLANO, G., RIVEROS, J., FERNÁNDEZ-VAREA, J. & SALVAT, F. (1996). Scanning, Monte Carlo simulation of electron backscattering in solids using a general-purpose computer code. *Microscopy* **10**, 625–638.

ACOSTA, E., LLOVET, X., COLEONI, E., RIVEROS, J.A. & SALVAT, F. (1998). Monte Carlo simulation of X-ray emission by kilovolt electron bombardment. *J Appl Phys* **83**(11), 6038–6049.

Acosta, E., Llovet, X. & Salvat, F. (2002). Monte Carlo simulation of bremsstrahlung emission by electrons. *Appl Phys Lett* **80**, 3228–3230.

Galván Josa, V., Bertolino, S.R., Riveros, J.A. & Castellano, G. (2009). Methodology for processing backscattered electron images. Application to Aguada archaeological paints. *Micron* **40**, 793–799.

Ginibre, C., Kronz, A. & Wörner, G. (2002). High-resolution quantitative imagining of plagioclase composition using accumulated backscattered electron images: New constraints on oscillatory zoning. *Contrib Mineral Petrol* **142**, 436–448.

Goldstein, J., Newbury, D., Echlin, P., Joy, D., Romig, A., Lyman, C., Fiori, C. & Lifshin, E. (1992). *Scanning Electron Microscopy and X-Ray Microanalysis: A Text for Biologists, Materials Scientists, and Geologists*, pp. 69–147. New York: Plenum Press.

Harding, D.P. (2002). Mineral identification using a scanning electron microscope. *Miner Metallurg Proc* **19**, 215–219.

Joy, D.C. (1991). Contrast in high-resolution scanning electron microscope images. *J Microsc* **161**, 343–355.

Keune, K., Van Loon, A. & Boon, J.J. (2011). SEM backscattered-electron images of paint cross sections as information source for the presence of the lead white pigment and lead-related degradation and migration phenomena in oil paintings. *Microsc Microanal* **17**, 1–6.

Kjellsen, K.O., Monsøy, A., Isachsen, K. & Detwiler, R.J. (2003). Preparation of flat-polished specimens for SEM-backscattered electron imaging and X-ray microanalysis—importance of epoxy impregnation. *Cement Concrete Res* **33**, 611–616.

Llovet, X., Sorbier, L., Campos, C.S., Acosta, E. & Salvat, F. (2003). Monte Carlo simulation of X-ray spectra generated by kilo-electron-volt electrons. *J Appl Phys* **93**, 3844–3851.

Peters, C.A. (2009). Accessibilities of reactive minerals in consolidated sedimentary rock: An imaging study of three sandstones. *Chem Geol* **265**, 198–208.

Reed, S. (1993). *Electron Probe Microanalysis*, 2nd ed. Cambridge, UK: Cambridge University Press.

Reimer, L. (1993). *Image Formation in Low-Voltage Scanning Electron Microscopy*. Bellingham, WA: SPIE Optical Engineering Press.

Reuter, W. (1972). The ionization function and its application to the electron probe analysis of thin films. In *Proceedings 6th International Congress on X-ray Optics and Microanalysis*, Shinoda, G., Kohra, K. & Ichinokawa, T. (Eds.), pp. 121–130. Tokyo: University of Tokyo Press.

Roschger, P., Fratzl, P., Eschberger, J. & Klaushofer, K. (1998). Validation of quantitative backscattered electron imaging for the measurement of mineral density distribution in human bone biopsies. *Bone* **23**(4), 319–326.

Salvat, F., Fernández-Varea, J.M. & Sempau, J. (2003). PENELOPE. A code system for Monte Carlo simulation of electron and photon transport. OECD/NEA Data Bank, Issy-les-Moulineaux, France.

Schalm, O., Janssens, K. & Caen, J. (2003). Characterization of the main causes of deterioration of grisaille paint layers in 19th century stained-glass windows by J.-B. Capronnier. *Spectrochim Acta B* **58**, 589–607.

Sempau, J., Fernandez-Varea, J.M., Acosta, E. & Salvat, F. (2003). Experimental benchmarks of the Monte Carlo code penelope. *Nucl Instrum Meth B* **207**(2), 107–123.

Steel, R.G.D. & Torrie, J.H. (1960). *Principles and Procedures of Statistics*, pp. 187–287. New York: McGraw-Hill.

Triebold, S., Kronz, A. & Wörner, G. (2006). Anorthite-calibrated backscattered electron profiles, trace elements, and growth textures in feldspars from the Teide–Pico Viejo volcanic complex (Tenerife). *J Volcanol Geotherm Res* **154**, 117–130.